

# Comparison between past and future extreme precipitations simulated by global and regional climate models over the Tibetan Plateau

Yanhong Gao,<sup>a\*</sup>  Linhong Xiao,<sup>a</sup> Deliang Chen,<sup>b</sup> Jianwei Xu<sup>a,c</sup>  and Hongwen Zhang<sup>a</sup>

<sup>a</sup> Key Laboratory of Land Surface Process and Climate Change in Cold and Arid Regions, Northwest Institute of Eco-environment and Resources, Chinese Academy of Sciences, Lanzhou, China

<sup>b</sup> Department of Earth Sciences, Regional Climate Group, University of Gothenburg, Gothenburg, Sweden

<sup>c</sup> Department of Geographical Science, Hunan University of Arts and Science, Changde, China

**ABSTRACT:** Past studies on regional climate change over the Tibetan Plateau (TP) have mainly looked at changes in the mean climate. This study focuses on past and future extreme precipitations, simulated by global and regional climate models over the TP. To assess the influence of large-scale forcing on dynamic downscaling using Weather Research and Forecasting (WRF) model, downscaling results for the historical period (1980–2005) with ERA-Interim reanalysis and CCSM4 as forcings are evaluated against a gridded observational data set. These are inter-compared before future projections for the period 2005–2100 under two scenarios (RCP4.5 and RCP8.5). The followings are obtained: (1) the reanalysis greatly overestimates not only the mean, but also extreme precipitation. The overestimation in CCSM4 is even larger than that of the reanalysis. (2) The two downscalings outperform their forcings, reflected by reduced overestimation for extreme precipitation frequency, increased spatial pattern correlations and more accurate linear trends, especially for the downscaling driven by CCSM. This demonstrates the constraining power of the fine-scale modelling and the importance of more realistic representations of surface forcing and related processes in the TP. (3) CCSM4 projects a general wetting across the whole TP with increases of heavy precipitation as well as the wetting intensification with warming. WRF also projects an overall wetting, but the wetting is less sensitive to the warming and there is more of an increase in light precipitation frequency. More importantly, a diverse pattern with wetting in the north and drying in the south is found in the dynamical downscaling in contrast to the uniform wetting in its forcing.

KEY WORDS Tibetan Plateau; dynamic downscaling; extreme precipitation indices

Received 22 October 2016; Revised 16 July 2017; Accepted 18 July 2017

## 1. Introduction

General circulation models (GCMs) are the most important tools for estimating future climate under various scenarios of greenhouse gas emissions (Solomon *et al.*, 2007). However, the inability of GCMs – and advantages of regional climate models (RCMs) – in capturing characteristics at regional scales point to the necessity of downscaling the GCMs' output to finer scales. Dynamical downscaling often involves a RCM nested in a GCM. It is generally considered more reliable than a statistical downscaling approach due to the dynamical frames and physics processes included in RCMs, although it is more computer intensive and time consuming than the statistical one (e.g. Ji and Kang, 2013). These are particularly true for mountainous regions.

The Tibetan Plateau (TP) is the largest and the highest plateau in the world. It has rugged terrain, including a

series of mountain ranges with the highest over 8000 m. The heterogeneous terrain and complex topography are more realistically represented in a finer resolution grid system than coarse ones (Figure 1). With the low temperature climatology and a pronounced warming rate at about twice the global average in recent decades (Solomon *et al.*, 2007; Wu *et al.*, 2007; Hansen *et al.*, 2010), the extreme precipitation intensity over the TP was projected to increase along with the surface air temperature (Jiang *et al.*, 2012). If the ‘the wet gets wetter, and the dry drier’ pattern (e.g. Skliris *et al.*, 2016) is true at the regional scale, we should expect less precipitation in the northwestern TP and more precipitation in the southeastern TP during warming as the northwest area has an arid to semi-arid climate, and the southeastern a humid to semi-humid one. However, observed records over recent decades reveal an inverted change over the TP with increased precipitation in the northwest and a decrease in the southeast (Gao *et al.*, 2014, 2015a, 2015b).

Dynamic downscaling has been widely used to simulate past and future fine-scale climates in North America, Europe and East Asia. For instance, the North American Regional Climate Change Assessment Program

\*Correspondence to: Y. Gao, Key Laboratory of Land Surface Process and Climate Change in Cold and Arid Regions, Northwest Institute of Eco-environment and Resources, Chinese Academy of Sciences, Lanzhou, Gansu 730000, China. E-mail: gaoyh@lzb.ac.cn

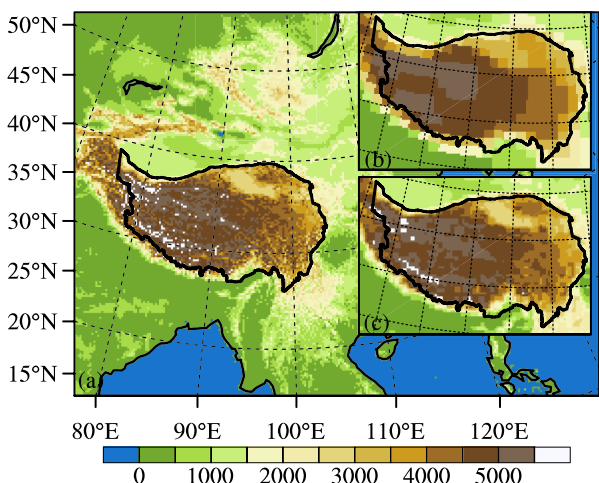


Figure 1. Simulation domain and topography in the dynamical downscaling and different resolution of the topography over the Tibetan Plateau (a) in CCSM (b) and WRF (c). [Colour figure can be viewed at [wileyonlinelibrary.com](http://wileyonlinelibrary.com)].

(NARCCAP) has been established to project the climate changes over North America. It found that RCMs' future projections are less sensitive to climate change than those from GCMs over the Colorado River basin (Gao *et al.*, 2011a, 2012b). The Coordinated Regional Climate Downscaling Experiment (CORDEX) is an international effort designed to objectively assess and inter-compare various regional climate downscaling techniques, providing solid scientific bases for impact assessments and other uses of downscaled climate information. In Asia, two regions were selected: South Asia and East Asia. Climate changes from regional climate downscaling have been assessed and evaluated widely over East Asia under the CORDEX framework (Gao *et al.*, 2002, 2012a, 2013; Li *et al.*, 2016; Tang *et al.*, 2016). The TP is located to the north of South Asia and west of the East Asia, not belonging to either region that CORDEX has focused on. Therefore, CORDEX leaves room for the TP to be in the focus. Besides CORDEX, a few regional dynamic downscaling projections over the whole of China and East Asia were reported (Gao *et al.*, 2011b; Xu *et al.*, 2012; Buccignani *et al.*, 2014; Ji and Kang, 2015; Bao *et al.*, 2015; Yu *et al.*, 2015; Guo and Wang, 2016). Most of them focus on the evaluations and projections of the annual mean surface air temperature and precipitation. The evaluation and projection of extreme precipitation over East Asia under a certain scenario of Coupled Model Intercomparison Project Phase 3 (CMIP3; Gao *et al.*, 2002; Tang *et al.*, 2016) and Phase 5 (CMIP5; Ji and Kang, 2015; Yu *et al.*, 2015) are mentioned in a few of them. Also, all of these focus on extreme event projections over the whole of China.

Recent studies have identified the spatial scale of climate variations over the TP (Gao *et al.*, 2015a; Chen *et al.*, 2016), which confirms the importance of having spatial resolutions finer than those used by GCMs to successfully simulate precipitation variations for the region. Further, Gao *et al.* (2015c) focus on the regional

dynamic downscaling analysis over the TP, finding that dynamic downscaling better captures elevation-dependent warming than the reanalysis that was used as large-scale forcing for the dynamic downscaling. The well-known significant overestimation of the precipitation over the TP (e.g. Su *et al.*, 2013) is also greatly constrained by the dynamic downscaling. It has been established that dynamic downscaling better captures the observed change patterns than reanalysis and GCMs (Gao *et al.*, 2015a), in which land surface processes play an important role (Gao *et al.*, 2017). Given the finer representation of the land surface characteristics and better performance of dynamic downscaling than its forcing, it is expected that dynamic downscaling also does a better job in projecting future climate changes on the regional scale than GCMs.

This work focuses on a comparison between GCM and RCM simulations of extreme precipitation over the TP throughout commonly used historic period and into the future. The comparison between model simulations and observations during the historical observation period can tell how the models perform for the study region and the target variable, which is useful for the interpretation of the differences between the future projections by the two models. The study proceeds as follows. Section 2 describes the data and methodology used. Section 3 evaluates the historical simulations of the two dynamic downscaling tools driven by a reanalysis and a GCM respectively, compared to observation and coarse-resolution forcing, as well as their future projections. Conclusions and discussions are found in Section 4.

## 2. Data and methodology

### 2.1. Large-scale forcings

Before commencing dynamic downscaling, GCM selection is an important step to reduce the potential for systematical errors being introduced to the RCM simulation. Xu *et al.* (2016) evaluated the performances of 14 CMIP5 GCMs for six variables used as dynamic downscaling inputs and found that CNRM-CM5 and CCSM are relatively superior to other GCMs not only in the spatial pattern aspect, but also in linear trends over the TP. Hence, CCSM4 was chosen as the forcing GCM for this study. It is called CCSM for short in the following texts and figures.

To evaluate biases from forcing, the ERA-Interim reanalysis (hereafter called ERAI) was also used as forcing in this study. ERAI is an improved version of the ERA-40 reanalysis. It has been proven best among the reanalysis products available in describing the temperature and water cycle over the TP (Wang and Zeng, 2012; Gao *et al.*, 2014). The horizontal resolution for CCSM and ERAI is  $0.9^\circ \times 1.25^\circ$  and  $0.7^\circ$  respectively.

### 2.2. Configuration of the dynamic downscaling

The Weather Research and Forecasting Model (WRF; <http://www.wrf-model.org/index.php>; Mesoscale and Microscale Meteorology Division, 2008) is utilized for the downscaling. WRF is a mesoscale numerical regional

climate prediction system which has been widely used in dynamic downscaling worldwide. For instance, the NARCCAP (Leung *et al.*, 2006) used WRF among four RCMs to produce high resolution climate scenarios for the United States, Canada and northern Mexico. It was also used as one of the RCMs in the CORDEX over East Asia and South Asia.

Dynamic downscaling simulations here were conducted for the historical period 1979–2005 driven by CCSM, and for 1979–2011 driven by ERAI. For the future period 2005–2100 under scenarios RCP4.5 and RCP8.5, WRF was driven by CCSM projection.

WRF configuration, including choices of physical parameterizations, followed previous dynamical downscaling over the TP (WRF1 in Gao *et al.*, 2017). The WRF WSM3 microphysics scheme and Grell–Devenyi ensemble convective scheme (Mesoscale and Microscale Meteorology Division, 2008) were used. They were designed for mesoscale simulation compared to schemes for large-scale simulation used in CCSM (Climate and Global Dynamics Division, 2010). Simulation domain covers nearly the whole Asian continent (Figure 1) with the horizontal resolution of 30 km. The historical simulations driven by CCSM and ERAI were initialized at 0000 UTC 1 January 1979 and ended at 2300 UTC 31 December 2005 and 2011 respectively. Projection runs were initialized at 0000 UTC 1 January 2005 and ended at 2300 UTC 31 December 2099. The first year (1979 and 2005) of the two periods was taken as the spin-up time and not used in the analysis. The lateral boundary conditions and SST were updated every 6 h and the simulation was outputted in 3 h interval.

### 2.3. Observational data

The gridded precipitation observations with a resolution of  $0.5^\circ \times 0.5^\circ$ , provided by the National Climate Center, China Meteorological Administration (CMA), are used as references for the historic simulation evaluations. The gridded data are based on observed precipitation from 2416 stations from 1961 to 2012 in China. They were generated by an optimum interpolation method based on a climatological background field which can substantially reduce analysis errors arising from precipitation heterogeneity (the National Meteorological Information Center, 2012). Orographic effect on precipitation has also been considered in the interpolation (Shen *et al.*, 2010), referred to here as OBS.

### 2.4. Precipitation indices

The precipitation indices used are based on the definitions recommended by the CCI/CLIVAR/JCOMM Expert Team on Climate Change Detection and Indices (e.g. Zhang *et al.*, 2011). The main function of these indices is to support evaluating the changes in the intensity, frequency and duration of precipitation events and temperatures in observations and model simulations (e.g. Ou *et al.*, 2013). The precipitation indices used in this study are listed in Table 1. Maximum number of consecutive dry CDD and Maximum

Table 1. List of the nine precipitation indices used in this study, based on the recommendation of the CCI/CLIVAR/JCOMM Expert Team on Climate Change Detection and Indices (ETC-CDI; [www.climdex.org/indices.html](http://www.climdex.org/indices.html)).

Indices	Definition	Units
CDD	Maximum number of consecutive dry ( $RR < 1 \text{ mm}$ ) days	Days
CWD	Maximum number of consecutive wet ( $RR \geq 1 \text{ mm}$ ) days	Days
R1	Annual count of days when $RR \geq 1 \text{ mm}$	Days
R10	Annual count of days when $RR \geq 10 \text{ mm}$	Days
R20	Annual count of days when $RR \geq 20 \text{ mm}$	Days
SDII	Simple precipitation intensity index (wet day mean)	$\text{mm day}^{-1}$
Rx1	Maximum 1-day precipitation	mm
Rx5	Maximum consecutive 5-day precipitation	mm
PTOT	Annual total precipitation in wet days	mm

number of consecutive wet CWD present the duration of dry/wet events. R1, R10 and R20 present frequency of precipitation events with a certain precipitation amount. SDII, Rx1 and Rx5 denote the intensity of the precipitation events. Annual total precipitation in wet days PTOT denotes the total annual precipitation.

### 2.5. Methodology

Dowscaled extreme precipitation projections driven by a GCM under representative concentration pathway (RCP) 4.5 and 8.5, relative to the historical period, are analysed in this study. The high-resolution simulation projections are compared with their driving GCMs. Given the fact that GCMs possess systematic biases, which could be transferred and therefore affect the downscaling results, it is necessary to evaluate the impact of these in the historical period before future projection. Reanalysis is usually taken as ‘true data’ for the historical period due to the use of multi-source observations and assimilation processes. To assess the impact of GCM biases on downscaling results, extreme precipitation simulations in ERAI, CCSM and WRF dynamical downscalings are first assessed for the historical period (1980–2005). Then, the future projections for the near- (2016–2035) and long-term (2081–2100) compared to a historical period of 20 years (1986–2005) are analysed. To facilitate comparisons among the forcing data from ERAI, CCSM, WRF and OBS with different resolutions, all modelled indices were interpolated into  $0.5^\circ \times 0.5^\circ$  resolutions, the same as the OBS. Model performance in the historical period is evaluated by comparing the simulated indices with those observed. BIAS, standard deviation (SD), root-mean-square-error (RMSE) and spatial correlation coefficients (SCCs) were calculated to quantify the differences. For the projection, the relative changes compared to the historical climatology are calculated

and compared between the downscaling and CCSM simulations.

### 3. Results and discussion

#### 3.1. Evaluation for the historical period

##### 3.1.1. Climatology

Table 2 summarizes the annual mean and SD of the nine indices averaged over the TP for the OBS, two forcings and two WRF simulations in the historical period 1980–2005. It also illustrates the relative biases and pattern correlation coefficients between the observation and simulations. All these precipitation indices are overestimated except for CDD and Rx5 in ERAI, and its forced WRF simulation. Larger relative biases exist in the overestimation of precipitation frequency than the intensity and PTOT. The heavier the precipitation, the larger the overestimation. It is the highest in R20. At its maximum, it reaches five times the OBS in CCSM. ERAI overestimates R20 by 258%. The great overestimation was constrained in the downscalings using WRF. The lighter the rainfall, the less chance for overestimation in WRF compared to its forcing. The greatest reduction of the relative biases in WRFs lies in R1 and CWD as well as PTOT, especially for the WRF simulation driven by CCSM, which is smaller than one-third of the biases in the forcing. However, no consistent reduction of the overestimation in the forcing is found in precipitation intensity-related variables SDII, Rx1 and Rx5.

OBS shows the highest frequency of light precipitation (less than 1 mm day<sup>-1</sup>) occurrence. The higher the precipitation intensity, the lower the frequencies (Figure 2(a)). All the model simulations underestimate light precipitation frequency; however, there is an overestimation in frequencies for heavier precipitation with intensity higher than 1 mm day<sup>-1</sup>. The highest overestimation occurs in the intensity interval of 1–4 mm day<sup>-1</sup>. Larger spread occurs in the intensity interval of 4–7 mm day<sup>-1</sup>. CCSM overestimates the most. ERAI ranks second following the simulations with WRFs driven by ERAI and CCSM. Despite having the highest frequency for light precipitation, observed PTOT is highest for rainfall intensity in the range of 1–4 mm day<sup>-1</sup>. ERAI and CCSM both capture the PTOT for light rainfall, but overestimate the PTOT for other intensities. It reaches the highest with 4–7 mm day<sup>-1</sup> (Figure 2(c)). WRF simulated PTOT variation is consistent with the OBS, showing the highest in 1–4 mm day<sup>-1</sup>. The highest overestimation for 4–10 mm day<sup>-1</sup> in the forcing is passed over to WRF. Apparently, the overestimation in PTOT mainly comes from the overestimation in the frequencies of middle rainfall intensities (Figure 2(a)).

#### A. CDD and CWD

Figure 3 presents the climatology of the nine observed and simulated precipitation indices over the TP in the historical period 1980–2005. The observed CDD shows a high centre in the northwestern TP and a low in the southeastern TP, reflecting on the fact that there is a severer

Table 2. Annual means (mean) and SD of the nine precipitation indices averaged over the TP which were calculated based on observations (OBS), ERAI–Interim reanalysis (ERAI), Global climate simulation (CCSM), and regional downscaling driven by ERAI (WRF\_ERAI) and CCSM (WRF\_CCSM) (units: the former five in days; SDII in mm day<sup>-1</sup>; the last three in mm) during 1980–2005.<sup>a</sup>

	SCC																		
	Mean				SD				Relative bias (%)										
	OBS	ERAI	CCSM	WRF <sub>–</sub> ERAI	OBS	ERAI	CCSM	WRF <sub>–</sub> ERAI	OBS	ERAI	CCSM	WRF <sub>–</sub> ERAI							
CDD	77.2	54.8	28.5	47.6	51.5	6.86	7.07	4.28	3.92	5.63	-29	-63	-38	-33	0.8	0.8	0.4	0.5	0.5
CWD	9.9	24.5	26.3	16	15.2	0.92	3.39	1.89	1.39	1.78	148	166	62	54	0.5	0.4	0.4	0.4	0.4
R1	79.2	132.3	162.9	110.3	103.3	3.64	9.71	6.12	4.44	4.14	67	106	39	30	0.8	0.7	0.7	0.7	0.7
R10	9.2	21.5	24.5	19.8	17.6	0.83	6.12	1.3	1.31	1.25	135	168	117	92	0.7	0.6	0.6	0.6	0.7
R20	1.6	5.7	7.8	5.5	4.7	0.22	2.18	0.65	0.58	0.49	258	392	244	194	0.5	0.6	0.6	0.6	0.7
SDII	4.4	5.2	5.5	5.7	5.6	0.18	0.67	0.16	0.21	0.18	19	25	31	27	0.6	0.5	0.7	0.7	0.7
Rx1	22.2	28.7	36.3	33.2	32.6	1.43	5.13	2.03	1.56	1.6	29	64	49	47	0.6	0.6	0.7	0.7	0.7
Rx5	46.5	28.7	87	33.2	70.8	3.31	5.13	7.13	1.56	4.34	-38	87	-29	52	0.6	0.6	0.7	0.7	0.7
PTOT	382.3	819.3	975.3	704.6	639.1	23.25	155.96	36.75	39.3	35.34	114	155	84	67	0.7	0.6	0.8	0.7	0.7

<sup>a</sup>Also, the relative biases of two forcings and two WRFs with respect to OBS, SCC between the four simulations and OBS for their climatology over the TP are shown.

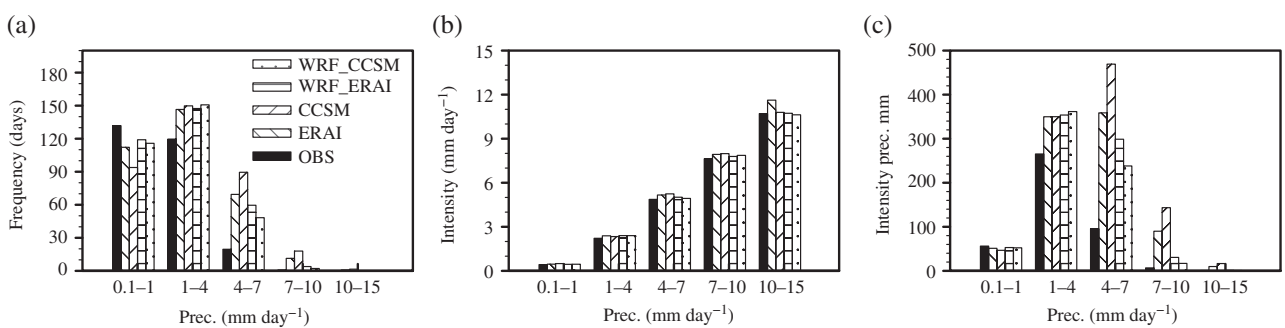


Figure 2. Observed (OBS), two forcings (ERA1 and CCSM) and two WRF simulated historical precipitation frequency (a), intensity (b) and total precipitation (c) on the annual basis for various precipitation intensity intervals observed from 1980 to 2005.

arid climate towards the northwestern TP (Figure 3(a1)). The driest area is located in the Chaidam basin. The second driest is found in the southwestern TP. ERA1 captures the two dry centres quite well but with a smaller areal coverage (Figure 3(b1)). CCSM not only heavily underestimates CDD, but also misses all the centres in its simulation (Figure 3(c1)). WRF captures the dry centre in the Chaidam basin just as ERA1 does, which is much better than CCSM; however, both dynamical downscalings lose the second centre over the southwestern TP (Figures 3(d1)–(e1)). Overall, these result in a higher, more realistic CDD average over the TP in WRF than CCSM (Table 2). Consequently, WRF better reproduces the observed CDD pattern with a higher spatial correlation than CCSM (Table 2). However, these improvements in CDD do not hold true compared with ERA1 (Table 2 and Figures 3(a1)–(e1)).

Observed CWD shows an opposite climate pattern to the CDD (Figures 3(a2) and (a1)). Observed CDD and CWD present consistent dryness and wetness change patterns over the TP, with an arid/semi-arid climate in northwest TP and humid/semi-humid climate in southeastern TP. ERA1 and CCSM both greatly overestimate CWD in the southern TP and Kunlun Mountains in CCSM. CWD simulated by CCSM is triple the OBS (Table 2). Overestimation of the CWD in ERA1 and CCSM is greatly reduced in WRF (Table 2 and Figures 3(b2) and (c2)). The great overestimation of CWD in the GCM over the TP is largely constrained in the dynamical downscaling, which is consistent with the findings about mean climates from previous studies (Gao *et al.*, 2015b).

### B. Precipitation frequency

Precipitation frequencies with daily precipitation amount to larger than or equal to 1, 10 and 20 mm (R1, R10 and R20) are shown in Figures 3(a3)–(e5) correspondingly. Observation shows less than 2 days for R20, and about 10 and 80 days for R10 and R1, respectively. The heavier the precipitation, the smaller areal coverage over the southeastern TP (Figures 3(a3)–(a5)). This is understandable as heavy precipitation occurs in the humid southeastern TP less often than the light rains. ERA1 and CCSM simulate a two- to fourfold increase of the OBS for R10 and R20 (Table 2). This demonstrates that

much higher heavy precipitation frequencies are simulated with the coarse-resolution models, especially over the southeastern edge with abrupt relief and abundant moisture flux brought about by the summer monsoon (Figures 3(b3)–(c5)). Double the volume of light rain is also simulated in CCSM. The overestimation in precipitation frequency in ERA1/CCSM is better constrained in the WRF simulations. A notable improvement with downscaling is the WRF simulated R1 with one-third in its forcing (Figures 3(e3) and (c3)). Moreover, pattern correlations for R20 and R10 between WRF and OBS are higher than their forcings, especially CCSM (Table 2). Although WRF, ERA1 and CCSM simulate a similar R1 pattern correlation with the OBS (Table 2), the fine-scale distribution of R1 caused by terrain is better represented in WRF than in the forcings (Figures 3(b3) and (e3)).

### C. Precipitation intensity

Observed precipitation intensities (SDII, Rx1 and Rx5) on the annual basis are  $4.4 \text{ mm day}^{-1}$ ,  $22.2 \text{ mm}$  and  $46.5 \text{ mm}$ , respectively (Table 2). ERA1 and CCSM both reasonably capture the historical precipitation intensity pattern with SCC higher than 0.5 (Table 2 and Figure 3). CCSM greatly overestimates the intensity of heavy precipitation events than ERA1. This is expected as reanalysis is constrained by observations and GCMs are far from perfect. ERA1 also slightly overestimates SDII and Rx1, but not for Rx5. Following the forcing, WRF also overestimates precipitation intensity with the exception of Rx5 driven by ERA1. However, the overestimation/underestimation is reduced when compared to CCSM and ERA1, although the difference between ERA1 and WRF is smaller than the difference between the CCSM and WRF. Precipitation is redistributed in the WRF simulations to have higher spatial correlations with OBS than their forcings (Table 2 and Figures 3(a6)–(e8)).

### D. PTOT

Observed PTOT is 382.3 mm averaged over the TP with more than 1200 mm in the southeastern TP and less than 200 mm in the western TP (Table 2 and Figure 3(a9)). ERA1 and CCSM remarkably overestimate with PTOT, being equal to 819.3 and 975.3 mm respectively (Table 2).

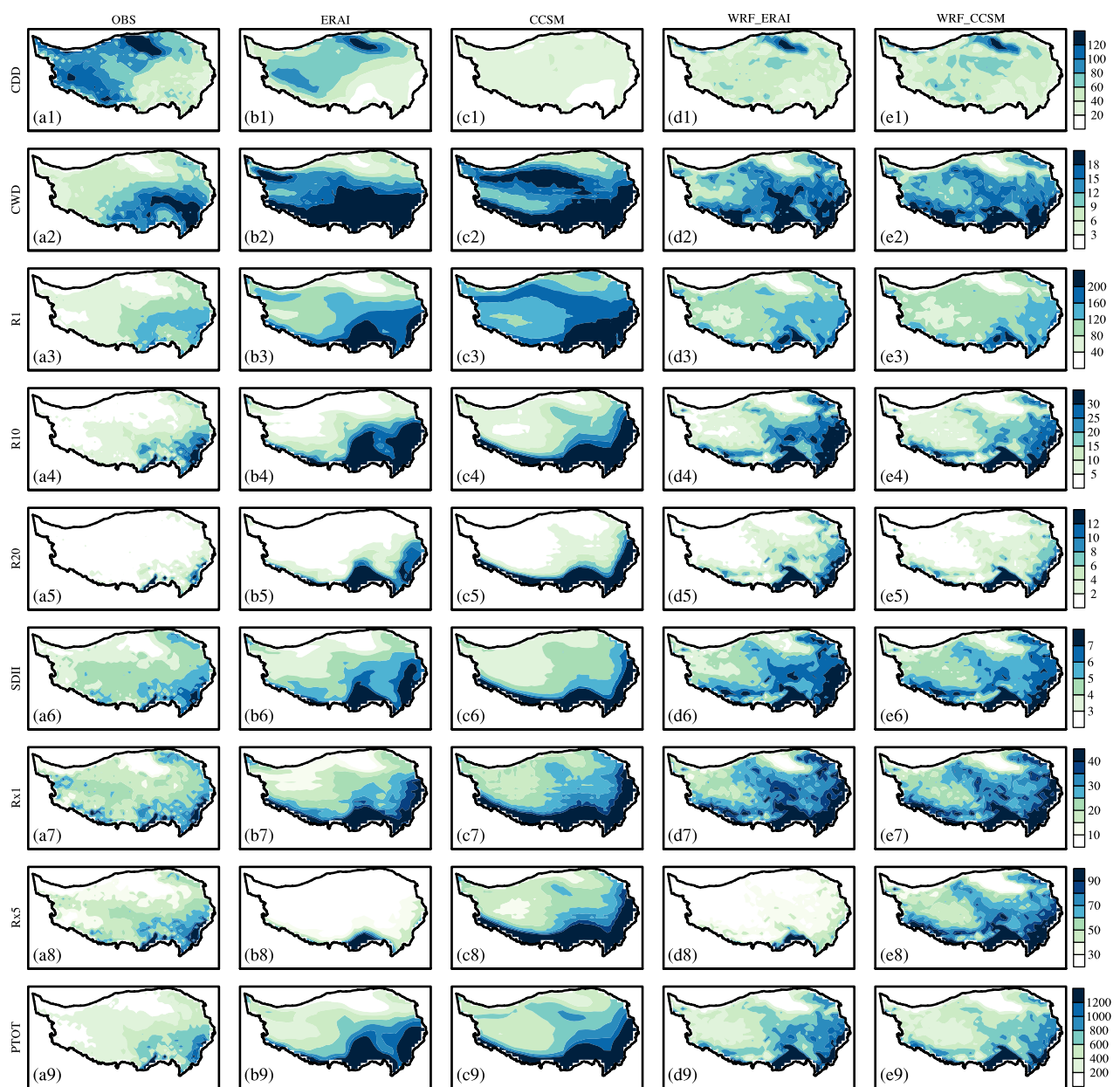


Figure 3. Distribution of the historical climatology (1980–2005) for the nine extreme precipitation indices over the TP calculated based on the observational data (a1–a9), two forcings (b1–c9) and two WRF simulations (d1–e9) (units: the former five in days; SDII in  $\text{mm day}^{-1}$ ; the last three in mm). [Colour figure can be viewed at wileyonlinelibrary.com].

The greatest overestimation is found in the humid southeastern periphery (Figures 3(b9)–(c9)) in both forcings, and those in CCSM are constrained in WRF (Figure 3(e9)). The pattern correlations between WRF and OBS are higher than those in ERAI and CCSM. Interestingly, the lowest PTOT centre at the Chaidam basin is better reproduced by WRF than CCSM, indicating the importance of fine resolution land surface forcing, especially with regard to the topography of arid conditions in the basin.

Taylor diagrams illustrate the improvements in precipitation indices simulated in WRF compared with ERAI and CCSM (Figure 4). The RMSE is highly reduced and the correlation is also slightly increased. The most notable improvements are found for CWD, R20 and PTOT. R10 and the three intensity indices additionally show a

reduction of RMSE in WRF compared to CCSM, but not compared to ERAI. Comparing two WRF simulations driven by ERAI and CCSM, we find a similar performance although greater biases exist in CCSM than ERAI. This indicates that the large biases in the GCMs forcing could be greatly constrained in WRF simulation to reach a comparable performance with the one driven by the reanalysis. It adds confidence for downscaling driven by CCSM to be used in future projections.

### 3.1.2. Linear trends over the historical period

OBS presents slight wetting trends over most of the TP for all indices except for Rx1 (Figures 5(a1)–(a9)). At the same time, ERAI greatly overestimates the wetting trends

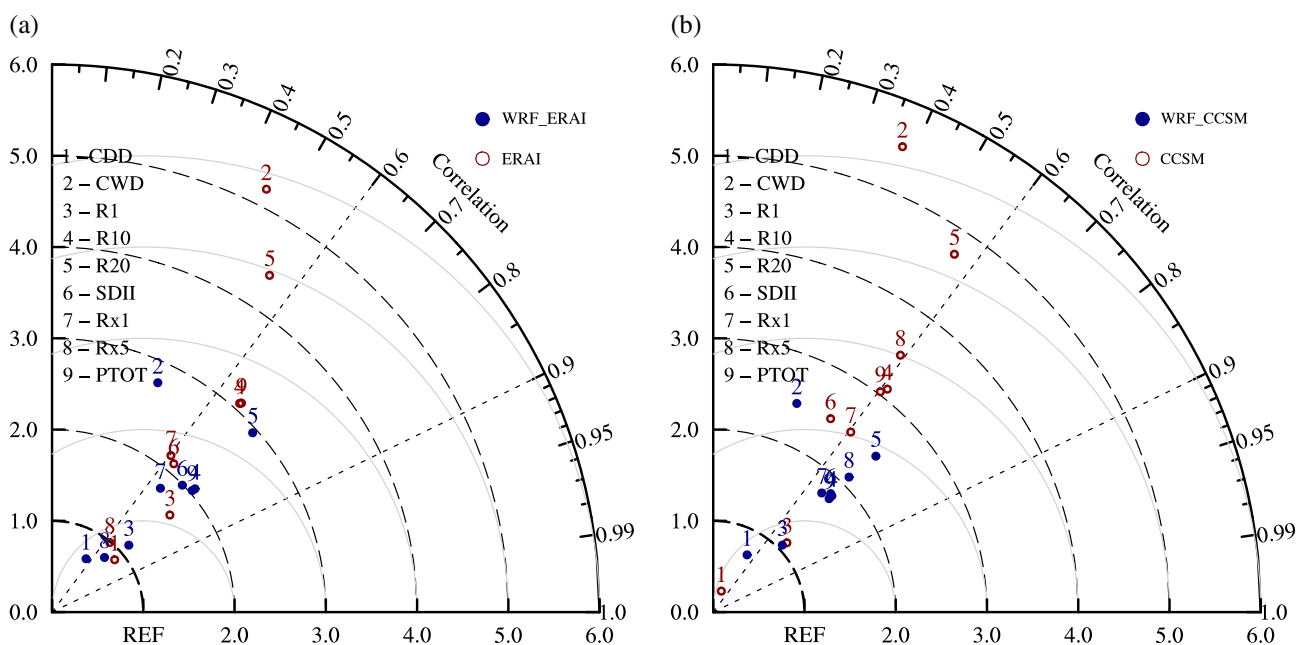


Figure 4. Taylor diagram of the historical climatology (1980–2005) of the nine precipitation indices for (a) ERAI and ERAI\_WRF and (b) CCSM and CCSM\_WRF simulations. [Colour figure can be viewed at [wileyonlinelibrary.com](http://wileyonlinelibrary.com)].

for all indices (Figures 5(b1)–(b9)) which are greatly constrained in WRF driven by ERAI (Figures 5(d1)–(d9)). CCSM has a similar magnitude to the OBS. However, it shows some exaggerated drying trends over the southern periphery. The change in precipitation in CCSM was redistributed to a more reasonable spatial pattern by the high-resolution simulation (Figures 5(e1)–(e9)). In general, WRF adds values in terms of the magnitude and spatial pattern in the linear trends over the historical period compared to their forcings.

Despite the similarity in linear trend patterns of the two downscalings over the TP, it is worth noting that the linear trend of CDW in WRF\_CCSM shows differences with CCSM in the southwestern TP (so was in R10, RX1 and RX5), but those driven by ERAI show similar trends as the boundary conditions provided by ERAI. It can be anticipated that linear trends in dynamical downscaling are dictated by large-scale forcing provided by GCMs. However, it is necessary to note that the RCM used in dynamical downscaling only receives information about the large-scale forcing at the boundary of the RCM which has its own dynamics within its computing domain. If constraints from the large-scale forcing are not strong enough and/or the difference between RCM and GCM processes are large, the RCM simulations will rely heavily on its model physics, land surface physics and surface characteristics. This is especially true over complex land terrain such as in mountainous regions. In our study over the Tibet, the downscaling with WRF may have produced more realistic local circulation over the TP, especially the ascending and downward motions related to the precipitation due to the finer resolution. Hence, the land surface forcing seems to play a more important role than the large-scale forcing in this complicated region, although

large-scale forcing is still a significant factor when it comes to linear trends at the local scale. In the end, it is the combined effects of the land surface and large-scale forcings that result in differences in the southwestern TP between the downscalings and forcings.

Averaged over the TP, ERAI presents larger interannual SDs for all indices than other data sets (SD in Table 2). Particularly, precipitation intensity indices and PTOT in ERAI are 6–10 times that of OBS. These large variations in ERAI are greatly constrained in WRF\_ERAI, which are no more than twice OBS. All indices except for CDD in CCSM show larger SD than OBS. Although Rx5 is even greater than ERAI, it is greatly constrained in WRF\_CCSM. On average, downscalings exhibit closer interannual variation with OBS than their forcings. Significant improvements appear in WRF\_ERAI compared to ERAI. A comparison among various RMSEs demonstrates the same as SDs (not listed).

It is also worth noting that the gridded reference data set utilized in the historical period evaluation is a result of interpolation from available station observations (Shen *et al.*, 2010). It is well-known that this mountainous region has a small number of these (e.g. Zhang *et al.*, 2017). The sparseness of observation in the western TP causes a great uncertainty in the interpolated gridded data set.

### 3.2. Future projections

Performance of WRF\_CCSM gives us some confidence for the future projection. CCSM and WRF\_CCSM projections for the near- (2016–2035) and long-term (2081–2100) future changes in relation to the historical period 1986–2005 under climate change scenarios RCP4.5 and RCP8.5 are summarized in Table 3.

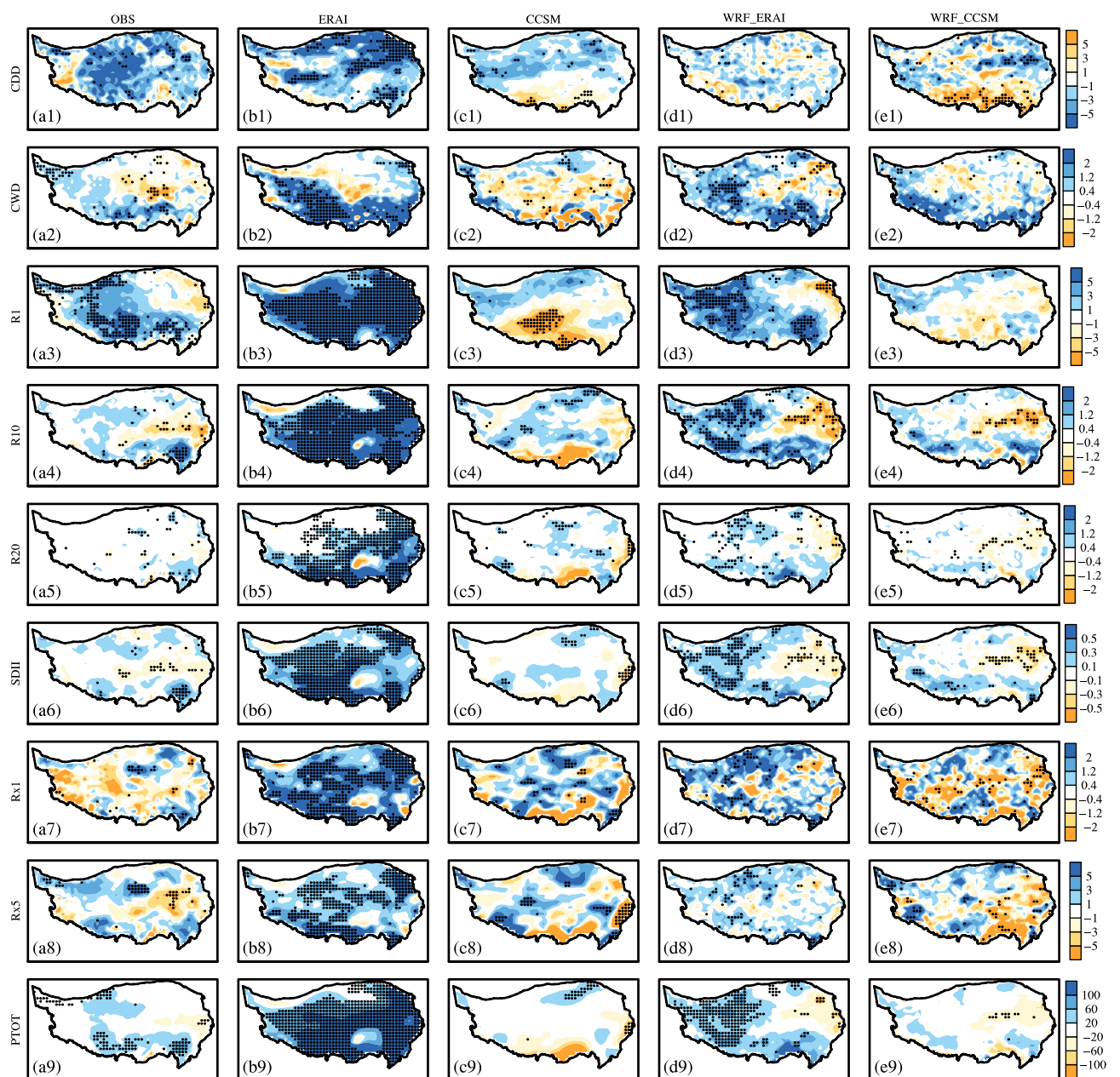


Figure 5. Distributions of the linear trends (units: the former five in days 10a-1; SDII in  $\text{mm day}^{-1}$  10a-1; the last three in  $\text{mm 10a-1}$ ) of the nine precipitation indices over the historical period (1980–2005), calculated for the observation (OBS), the two forcing (ERAI/CCSM) and two WRF simulations. [Colour figure can be viewed at wileyonlinelibrary.com].

### 3.2.1. Projections for the near-term future

Figure 6 shows the distribution of the relative changes over the TP for the short-term future. Under scenario RCP4.5, CCSM projects an increase in dry spell duration (CDD) by 1.0% and a decrease in wet spells (CWD) by 1.4%. WRF predicts almost no changes for both CDD and CWD. Spatially, CCSM projects longer dry durations in the central TP, whereas WRF simulates longer wet durations in the north and drier durations in the south (Figures 6(a2) and (b2)).

For the precipitation frequencies, CCSM projects 1.5, 4.1 and 7.4% increases for R1, R10 and R20 (Table 3) respectively. Although local relative changes reach as high

as 90% (R20 for CCSM because of the smaller denominator) (Figure 6(a5)), the average changes over the TP are smaller than 8%. The western TP is projected to experience more wetting changes than the eastern TP. WRF projects a similar magnitude change in R1 averaged over the whole TP as CCSM, with more wetting in the northern TP. For R10 and R20, WRF projects negative changes averaged over the TP.

A difference between CCSM and WRF is also found in precipitation intensity projection. CCSM projects increases in SDII, Rx1 and Rx5 (Table 3). However, WRF projects slight decreases in SDII and Rx1 as well as almost no change in Rx5.

Table 3. Projected relative changes (%) of the nine precipitation indices averaged over the TP in the near-term (2016–2035) and long-term future (2081–2100) compared to 1986–2005 for CCSM and WRF\_CCSM simulations under the RCP4.5 and RCP8.5 scenarios (units: %).

	2016–2035				2081–2100			
	RCP4.5		RCP8.5		RCP4.5		RCP8.5	
	CCSM	WRF	CCSM	WRF	CCSM	WRF	CCSM	WRF
CDD	1.0	0.3	−7.1	−4.6	−2.4	−9.1	−4.4	−9.8
CWD	−1.4	0.3	−4.3	−1.2	−3.8	2.9	−9.0	0.1
R1	1.5	1.9	0.4	2.1	0.7	5.2	0.6	8.0
R10	4.1	−1.8	1.7	1.6	10.3	6.8	19.2	11.4
R20	7.4	−4.9	4.5	−0.1	18.7	2.5	37.9	8.3
SDII	2.1	−1.2	1.9	0.0	7.4	2.2	15.3	3.5
Rx1	5.2	−1.1	6.9	0.1	14.3	3.2	29.9	4.9
Rx5	4.1	0.1	7.0	1.5	12.2	5.7	23.5	6.6
PTOT	3.7	0.2	2.3	2.0	8.1	6.4	16.4	10.7

Because of the projected general increases both in frequency and intensity, CCSM projects an 3.7% increase in PTOT for the near-term future under scenario RCP4.5, while WRF projects almost no change in PTOT (Table 3) because the increase in the northern TP and decrease in the southern TP (Figure 6(b9)) cancel each other out. The converse change pattern in WRF is reflected in the increased R1 in the north and decreased R10.

Under scenario RCP8.5, CCSM projects larger decreases in CDD and CWD, larger increases in precipitation intensity and smaller increases in frequencies than those under RCP4.5. This suggests there would be more shorter, rare, but high intensity precipitation events under RCP8.5 than RCP4.5. Nevertheless, PTOT averaged over the TP under RCP8.5 increases less than under RCP4.5 due to the lower projected frequency. Compared to the CCSM projection under RCP8.5, WRF projects much smaller changes in the intensity indices except for R1 in response to warming. This means that more/less, light/heavy precipitation events are projected in WRF than CCSM under RCP8.5.

In short, WRF projects fewer changes than CCSM in the near-term future under either RCP4.5 or RCP8.5. A contrasting pattern between the north and south has been simulated by WRF, compared to the rather uniform wetting over the whole TP in its forcing under RCP4.5. More light rains and less heavy rains are projected in WRF than forcing under RCP8.5.

### 3.2.2. Projections for the long-term future

Compared to the near-term projection, surface air temperature would increase from around 2.0 to 5.0 °C under RCP4.5 and RCP8.5 respectively in the long-term future. This is much larger than the warming in the near-term future. At the same time, changes in the precipitation indices projected in the long-term future are larger than the near-term. All the precipitation frequencies and intensities are projected to increase over the entire TP with the exception of R1 in CCSM (Table 3 and Figures 7(a3)–(a9) and (c3)–(c9)). Significant increases would occur in R10, R20, Rx1 and Rx5. Increases under RCP8.5 are projected to be twice the changes under RCP4.5. The most significant changes lie in R20 and Rx1. R20 would increase by

37.0% and Rx1 by 30% in CCSM under RCP8.5 (Table 3). This indicates that CCSM projects heavier precipitation with greater intensities and higher frequencies in the long-term future. Thus, PTOT would increase by 8.1 and 16.4% respectively.

The great increases in CCSM total precipitation occur in intervals larger than 7 mm day<sup>−1</sup> (Figures 8(e) and (f)) because of frequency increases (Figures 8(a) and (b)) except for interval over 10 mm day<sup>−1</sup> for RCP8.5 (Figure 8(d)). WRF projects fewer changes in the precipitation frequencies than CCSM for intervals larger than 7 mm day<sup>−1</sup>, but more for intervals 1–7 mm day<sup>−1</sup> (Figures 8(a) and (b)). This implies that WRF projects more wet days with higher frequency for light rain, but lower frequency for heavy rain than CCSM.

For the number of consecutive dry/wet days, CCSM projects a larger decrease in CDD and CWD in the long-term future than the near-term under RCP4.5 and RCP8.5 (Table 3) over the whole TP (Figure 7). On the contrary, WRF projects a decreased CDD over the TP and increased CWD (Table 3), with a pattern of increase in the north and decrease in the south (Figures 7(b2) and (d2)). This is highly consistent with the increases of R1 in the northern TP (Figures 7(b3) and (d3)). As a result, PTOT presents more increases in the north than south. The changed pattern in PTOT in the long-term future projected by WRF is consistent with those by Ji and Kang (2015).

In short, the three characteristics of the near-term future changes between CCSM and WRF are repeated more in the long-term future. These are: (1) the magnitude of changes in WRF averaged over the TP is smaller than the large-scale forcing; (2) the diverse spatial pattern of change in WRF in terms of the contrast between the north and the south presents a contrast against the rather homogeneous changes in the forcing; and (3) there is more light precipitation and less heavy precipitation in WRF than in CCSM. In other words, less extreme heavy precipitation events are projected in the high-resolution simulation than its course-resolution forcing. Changes under RCP8.5 are larger than those under RCP4.5.

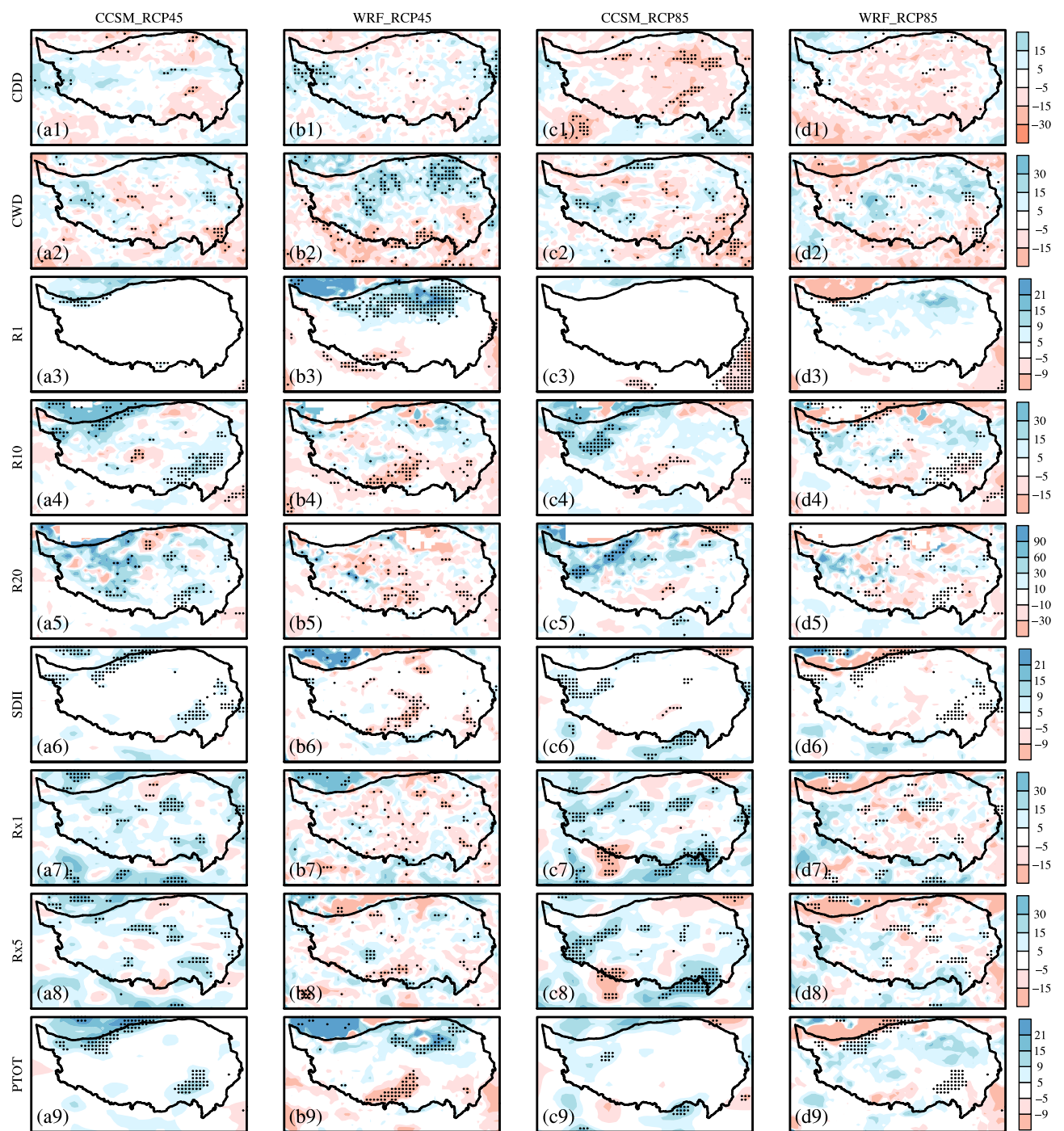


Figure 6. Relative changes (%) of the nine precipitation indices projected by CCSM (a, c) and WRF\_CCSM (b, d) in the near-term future (2016–2035) under the scenario of RCP4.5 (a, b) and RCP8.5 (c, d) compared to the historical period (1980–2005). Black dots denote changes that passed the two-tailed *t*-test with the statistical significant confidence level of 95%. [Colour figure can be viewed at wileyonlinelibrary.com].

#### 4. Summary

Dynamic downscaling using WRF driven by ERAI reanalysis and CCSM was applied to simulate past and future precipitation statistics over the TP. Nine precipitation indices from the dynamical downscaling were first evaluated with the help of a gridded observation data set. These results were also compared with their forcings for the historical climate conditions over the TP to demonstrate the added value of the downscaling. Finally, the future changes

in the nine precipitation indices under scenarios RCP4.5 and RCP8.5 were projected with WRF driven by CCSM4 projections.

ERAI and CCSM greatly overestimate the extreme and mean precipitation indices based on observations. This is more pronounced for the frequencies of the extreme rains. The large overestimations in precipitation frequency and amount in the reanalysis and CCSM are greatly constrained in the dynamical downscaling using WRF. Moreover, the dynamical downscaling is proven to be able

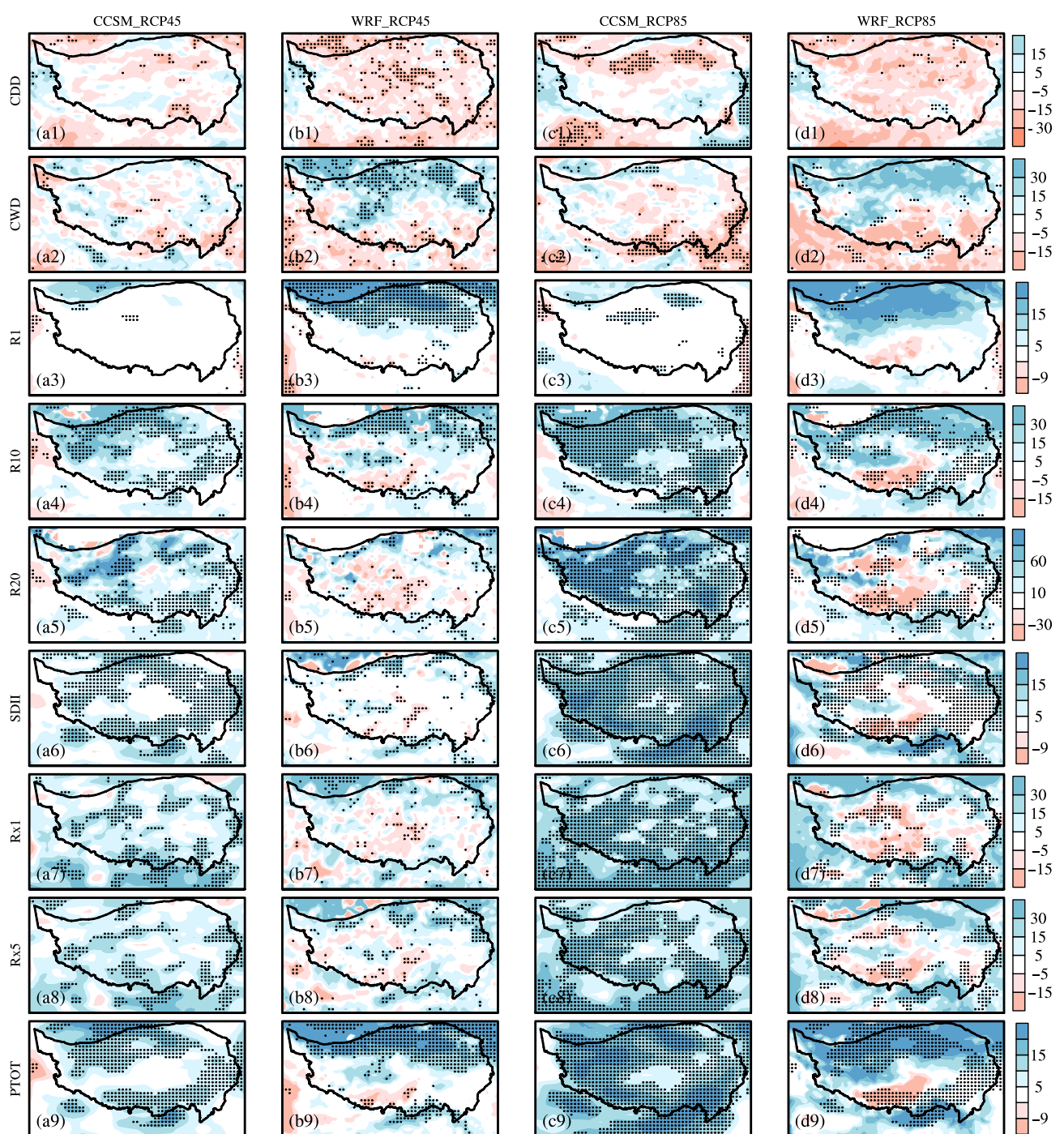


Figure 7. Relative changes (%) of the nine precipitation indices projected by CCSM (a, c) and WRF\_CCSM (b, d) in the long-term future (2081–2100) under the scenario of RCP4.5 (a, b) and RCP8.5 (c, d) compared to the historical period (1980–2005). Black dots denote the changes that passed the two-tailed *t*-test with the statistical significant confidence level of 95%. [Colour figure can be viewed at wileyonlinelibrary.com].

to better reproduce the historical spatial distribution of the precipitation intensities than its forcing. Further, the added values of the dynamical downscaling for linear trends of precipitation intensity could also be demonstrated for the CCSM and WRF\_CCSM pair during the historical period. It is also interesting to note that downscalings better present the observed interannual SDs than their forcings.

CCSM projects a general wetting over the entire TP in terms of the precipitation frequency, intensity, the number

of consecutive days for dry/wet spells and the PTOT with the exception of light rain frequency. Heavy precipitation frequency increases the most. The wetting increases with warmings either from RCP4.5 to RCP8.5, or from the near-term to the long-term future. WRF also projects more wetting under RCP8.5 than RCP4.5, but with three significant and interesting differences. First, the magnitude of changes in WRF is generally smaller than in the forcing averaged. Second, the WRF simulations show different signs for the changes in the north *versus* the south as was

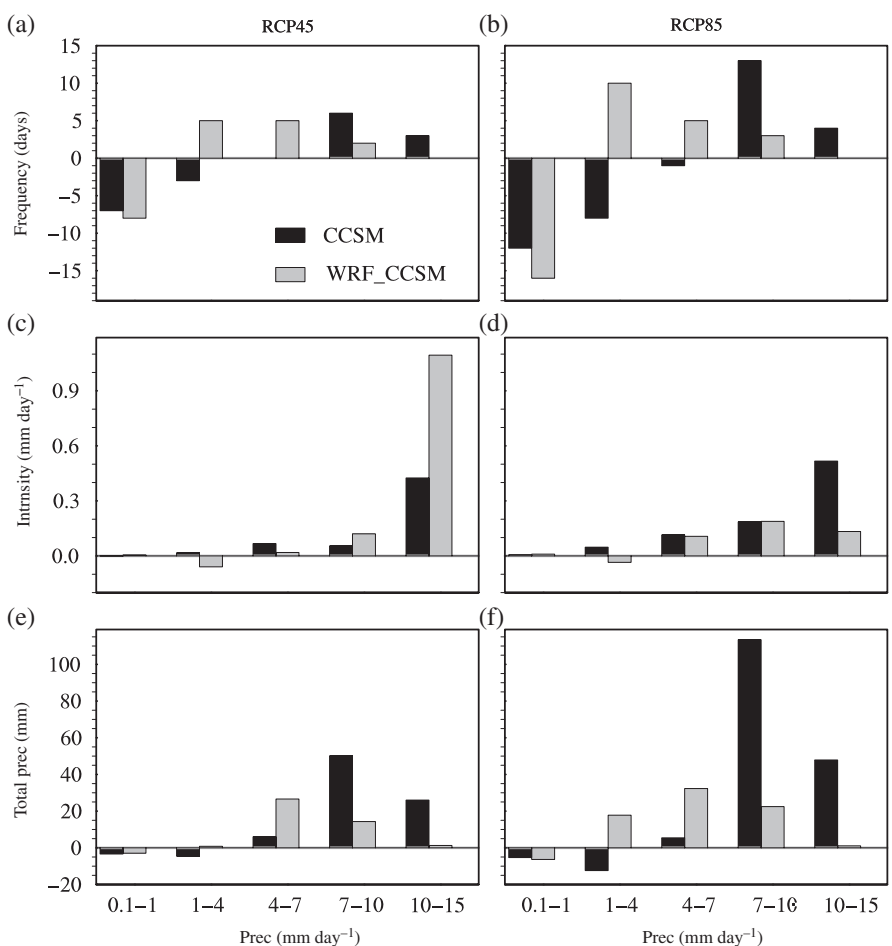


Figure 8. Changes of the precipitation frequency, intensity and total precipitation on an annual basis averaged across the whole TP for various precipitation intensity intervals for the long-term future (2081–2100) under the scenarios of RCP4.5 (a, c, e) and RCP8.5 (b, d, f) compared to the historical period (1980–2005).

the case for the historical period, while the CCSM projects rather uniform changes. Third, there is more light rain and less heavy rain in WRF than in CCSM projections.

In addition to the important role of the large-scale forcing for the dynamical downscaling, this study demonstrates that terrain and land characteristics can also play important roles. This is particularly true over the TP with its extremely complex terrain and land surface. Terrain in the southern TP possesses even higher heterogeneity than in the northern TP. Therefore, larger differences in projection between the coarse resolution GCM and the fine resolution downscaling also exist over the southern TP. This implies larger uncertainty in GCM projection over complex mountainous regions than areas with flat terrain.

## Acknowledgements

We appreciate the free access of the CMIP5 data sets, which are provided by the ESGF web portals (<http://pcmdi9.llnl.gov/esgf-web-fe/>). The observation data provided by the National Climate Center, China Meteorological Administration (CMA). This work is jointly supported by the Ministry of Science and Technology of the People's Republic of China (2013CB956004), and the

National Natural Science Foundation of China (91537105, 41322033). We thank the Supper-Computing Center of Chinese Academy of Science for computing the simulations. D. Chen is supported by Swedish VR, STINT, BECC and MERGE, as well as SNIC through S-CMIP.

## References

- Bao J, Feng J, Wang Y. 2015. Dynamical downscaling simulation and future projection of precipitation over China. *J. Geophys. Res. Atmos.* **120**(16): 8227–8243. <https://doi.org/10.1002/2015JD023275>.
- Bucignani E, Montesarchio M, Cattaneo L, Manzi MP, Mercogliano P. 2014. Regional climate modeling over China with COSMO-CLM: performance assessment and climate projections. *J. Geophys. Res. Atmos.* **119**(21): 12151–12170. <https://doi.org/10.1002/2014JD022219>.
- Chen D, Tian Y, Yao T, Ou T. 2016. Satellite measurements reveal strong anisotropy in spatial coherence of climate variations over the Tibet plateau. *Sci. Rep.* **6**: 30304. <https://doi.org/10.1038/srep30304>.
- Climate and Global Dynamics Division. 2010. Description of the NCAR Community Atmosphere Model (CAM 4.0). NCAR Technical Note. NCAR/TN-485+STR.
- Gao X, Zhao Z, Filippo G. 2002. Changes of extreme events in regional climate simulations over East Asia. *Adv. Atmos. Sci.* **19**(5): 927–942.
- Gao Y, Vano JA, Zhu C, Lettenmaier DP. 2011a. Evaluating climate change over the Colorado River basin using regional climate models. *J. Geophys. Res. Atmos.* **116**(D13): D13104. <https://doi.org/10.1029/2010JD015278>.

- Gao Y, Xue Y, Peng W, Hyun-suk K, Duane W. 2011b. Assessment of dynamic downscaling of the extreme rainfall over East Asia using a regional climate model. *Adv. Atmos. Sci.* **28**(5): 1077–1098. <https://doi.org/10.1007/s00376-010-0039-7>.
- Gao X, Shi Y, Zhang D, Wu J, Giorgi F, Ji Z, Wang Y. 2012a. Uncertainties in monsoon precipitation projections over China: results from two high-resolution RCM simulations. *Clim. Res.* **52**(1): 213–226. <https://doi.org/10.3354/cr01084>.
- Gao Y, Leung LR, Salathé EP, Dominguez F, Nijssen B, Lettenmaier DP. 2012b. Moisture flux convergence in regional and global climate models: implications for droughts in the southwestern United States under climate change. *Geophys. Res. Lett.* **39**(9): L09711. <https://doi.org/10.1029/2012GL051560>.
- Gao X, Wang M, Giorgi F. 2013. Climate change over China in the 21st century as simulated by BCC\_CSM1.1-RegCM4.0. *Atmos. Oceanic Sci. Lett.* **6**(5): 381–386. <https://doi.org/10.3878/j.issn.1674-2834.13.0029>.
- Gao Y, Cuo L, Zhang Y. 2014. Changes in moisture flux over the Tibetan Plateau during 1979–2011 and possible mechanisms. *J. Clim.* **27**(5): 1876–1893. <https://doi.org/10.1088/1748-9326/10/3/034013>.
- Gao Y, Leung LR, Zhang Y, Cuo L. 2015a. Changes in moisture flux over the Tibetan Plateau during 1979–2011: insights from a high-resolution simulation. *J. Clim.* **28**(10): 4185–4197. <https://doi.org/10.1175/JCLI-D-14-00581.1>.
- Gao Y, Li X, Leung LR, Chen D, Xu J. 2015b. Aridity changes in the Tibet plateau in a warming climate. *Environ. Res. Lett.* **10**(3): 034013. <https://doi.org/http://iopscience.iop.org/1748-9326/10/3/034013>.
- Gao Y, Xu J, Chen D. 2015c. Evaluation of WRF mesoscale climate simulations over the Tibetan Plateau during 1979–2011. *J. Clim.* **28**: 2823–2841. <https://doi.org/10.1175/JCLI-D-14-00300.1>.
- Gao Y, Xiao L, Chen D, Chen F, Xu J, Xu Y. 2017. Quantification of the relative role of land-surface processes and large-scale forcing in dynamic downscaling over the Tibetan Plateau. *Clim. Dyn.* **48**: 1705–1721. <https://doi.org/10.1007/s00382-016-3168-6>.
- Guo D, Wang H. 2016. Comparison of a very-fine-resolution GCM with RCM dynamical downscaling in simulating climate in China. *Adv. Atmos. Sci.* **33**(5): 559–570. <https://doi.org/10.1007/s00376-015-5147-y>.
- Hansen J, Ruedy R, Sato M, Lo K. 2010. Global surface temperature change. *Rev. Geophys.* **48**(4): RG4004. <https://doi.org/10.1029/2010RG000345>.
- Ji Z, Kang S. 2013. Double-nested dynamical downscaling experiments over the Tibetan Plateau and their projection of climate change under two RCP scenarios. *J. Atmos. Sci.* **70**(4): 1278–1290. <https://doi.org/10.1175/JAS-D-12-0155.1>.
- Ji Z, Kang S. 2015. Evaluation of extreme climate events using a regional climate model for China. *Int. J. Climatol.* **35**(6): 888–902. <https://doi.org/10.1002/joc.4024>.
- Jiang Z, Song J, Li L, Chen W, Wang Z, Wang J. 2012. Extreme climate events in China: IPCC-AR4 model evaluation and projection. *Clim. Change* **110**(1): 385–401. <https://doi.org/10.1007/s10584-011-0090-0>.
- Leung LR, Kuo Y, Tribbia J. 2006. Research needs and directions of regional climate modeling using WRF and CCSM. *Bull. Am. Meteorol. Soc.* **87**(12): 1747–1751. <https://doi.org/10.1175/BAMS-87-12-1747>.
- Li Q, Wang S, Lee D, Tang J, Niu X, Hui P, Gutowski WJ, Dairaku K, McGregor JL, Katzfey J, Gao X, Wu J, Hong S, Wang Y, Sasakik H. 2016. Building Asian climate change scenario by multi-regional climate models ensemble. Part II. Mean precipitation. *Int. J. Climatol.* **36**(13): 4253–4264. <https://doi.org/10.1002/joc.4628>.
- Mesoscale and Microscale Meteorology Division. 2008. A Description of the Advanced Research WRF Version 3, NCAR Technical Note. NCAR/TN-475+STR.
- Ou T, Chen D, Linderholm HW, Jeong J. 2013. Evaluation of global climate models in simulating extreme precipitation in China. *Tellus A* **65**(5): 1979. <https://doi.org/10.3402/tellusa.v65i0.19799>.
- Shen Y, Feng MN, Zhang HZ, Gao F. 2010. Interpolation methods of China daily precipitation data. *J. Appl. Meteorol. Climatol.* **21**(3): 279–286.
- Skliris N, Zika JD, Nurser G, Josey SA, Marsh R. 2016. Global water cycle amplifying at less than the Clausius–Clapeyron rate. *Sci. Rep.* **6**: 38752. <https://doi.org/10.1038/srep38752>.
- Solomon S, Qin D, Manning M. 2007. Climate change 2007: the physical science basis. In *Working Group I Contribution to the Fourth Assessment Report of the IPCC*. Cambridge University Press: New York, NY.
- Su F, Duan X, Chen D, Hao Z, Cuo L. 2013. Evaluation of the global climate models in the CMIP5 over the Tibetan Plateau. *J. Clim.* **26**(10): 3187–3208. <https://doi.org/10.1175/JCLI-D-12-00321.1>.
- Tang J, Li Q, Wang S, Lee D, Hui P, Niu X, Gutowski WJ, Dairaku K, McGregor J, Katzfey J, Gao X, Wu J, Hong S, Wang Y, Sasakik H. 2016. Building Asian climate change scenario by multi-regional climate models ensemble. Part I. Surface air temperature. *Int. J. Climatol.* **36**(13): 4241–4252. <https://doi.org/10.1002/joc.4628>.
- The National Meteorological Information Center. 2012. Assessment report of China monthly gridded surface air temperature version 2.
- Wang AH, Zeng XB. 2012. Evaluation of multireanalysis products with in situ observations over the Tibetan Plateau. *J. Geophys. Res.-Atmos.* **117**: D05102. <https://doi.org/10.1029/2011jd016553>.
- Wu S, Yin Y, Zheng D, Yang Q. 2007. Climatic trends over the Tibetan Plateau during 1971–2000. *J. Geogr. Sci.* **17**(2): 141–151. <https://doi.org/10.1007/s11442-007-0141-7>.
- Xu J, Shi Y, Gao X. 2012. Changes in extreme events as simulated by a high-resolution regional climate model for the next 20–30 years over China. *Atmos. Oceanic Sci. Lett.* **5**(6): 483–488. <https://doi.org/10.1080/16742834.2012.11447044>.
- Xu J, Gao Y, Chen D, Xiao L, Ou T. 2016. Evaluation of global climate models for downscaling applications centered over the Tibetan Plateau. *Int. J. Climatol.* **37**(2): 657–671. <https://doi.org/10.1002/joc.4731>.
- Yu E, Sun J, Chen H, Xiang W. 2015. Evaluation of a high-resolution historical simulation over China: climatology and extremes. *Clim. Dyn.* **45**: 2013. <https://doi.org/10.1007/s00382-014-2452-6>.
- Zhang X, Alexander L, Hegerl GC, Jones P, Tank AK, Peterson TC, Trewin B, Zwiers FW. 2011. Indices for monitoring changes in extremes based on daily temperature and precipitation data. *Wires Clim. Change* **2**(6): 851–870. <https://doi.org/10.1002/wcc.147>.
- Zhang C, Tang Q, Chen D. 2017. Recent changes in the moisture source of precipitation over the Tibetan Plateau. *J. Clim.* **30**: 1807–1819. <https://doi.org/10.1175/JCLI-D-15-0842.1>.